EFFECTIVE PLANE ARRANGEMENT OF DEEP MIXING PILES TO RESIST LATERAL FLOW OF LIQUEFIED GROUND

Hidenori Takahashi, Port and Airport Research Institute, Yokosuka, Japan, takahashi-h@pari.go.jp
Yoshiyuki Morikawa, Port and Airport Research Institute, Yokosuka, Japan, morikawa@pari.go.jp
Naoki Takahashi, Sumitomo-Mitsui Construction Co., Nagareyama, Japan, tnaoki@smcon.co.jp
Daiki Takano, Port and Airport Research Institute, Yokosuka, Japan, takano-d@pari.go.jp
Ikuo Towhata, University of Tokyo, Tokyo, Japan, towhata@geot.t.u-tokyo.ac.jp

ABSTRACT

The method in this study, in which cement-treated piles are installed into the ground to decrease the amount of liquefied lateral flow, has been studied. The authors are also investigating the most effective arrangement of piles to optimize cost-effectiveness. In their investigation, they propose shifting the position of the piles to prevent lateral flow in various directions. The present study conducted centrifuge model tests to clarify the improvement effect of piles against the lateral flow of liquefied soil and the effect of the pile arrangement. Then, numerical fluid analyses were conducted to consider the improvement mechanism. As a result, the model tests and numerical analyses showed that the pile improvement dramatically reduced the lateral displacement and that the average total flow velocity decreased in the irregular case.

Keywords: deep mixing pile, liquefaction, lateral flow, pile arrangement

INTRODUCTION

Liquefied ground subjected to seismic motion loses its stiffness and strength, and lateral flow often occurs in sloping areas and backfill areas behind collapsed quay walls. In the Hyogoken–Nanbu Earthquake in 1995, the reclaimed island that was surrounded by collapsed quay walls expanded toward the sea and the amount of displacement reached a few metres (Hamada et al., 1996). Two countermeasures can be considered to guard against lateral flow: preventing liquefaction and reducing lateral displacement. The former method is ideal; however it is costly and time-consuming. Based on these considerations, the authors (Takahashi et al., 2013; Morikawa et al., 2014) are currently studying a method in which cement-treated piles are installed into the ground (see Fig. 1) to decrease the amount of liquefied lateral flow. The countermeasure cost using this method is relatively low because of the low replacement ratio. The authors are also investigating the most effective arrangement of piles to optimize cost-effectiveness. It has been proposed that the position of the piles should be shifted so that lateral flow can be prevented in various directions, as described in Fig. 2.

Fig. 1 Cement-treated piles

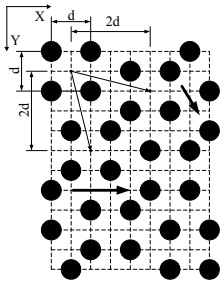

Fig. 2 Irregular pile arrangement

In the present study, a series of centrifuge model tests were implemented to clarify the efficacy of the pile improvement and the influence of the piles' arrangement. In ground flow, model piles were arranged in two patterns: regular and irregular. Then, numerical fluid analyses were conducted to consider the

improvement mechanism and the cause generating the difference in the two patterns of arrangement. Analyses simulated the centrifuge model tests as a first step by modelling the fully liquefied ground as the Newtonian fluid. Then, the flow properties were investigated in detail to examine the improvement mechanism.

CENTRIFUGE MODEL TESTS

Prepared model ground

Fig. 3 shows the vertical cross sections and top views of the representative test cases, which are summarized in Table 1. The first case, consisting of the unimproved sloping ground, was used to assess the viscous coefficient of fully liquefied ground for use in numerical analyses. In this case, the liquefiable sandy ground with a thickness of 100 mm – corresponding to 5 m in a prototype scale – was accumulated on the non-liquefiable dense sandy layer. The inclination of the slope was set to be 1/10. Tests on the other cases that included improvement piles were conducted to investigate the effect of piles on liquefied ground flow. By changing the arrangement of the piles, the different effects induced by the arrangement were assessed. One arrangement was a regular type, and the other was an irregular type in which the position of the piles was shifted to consider four piles as a pair. In these cases, a thick liquefiable sandy ground was placed on the non-liquefiable layer. The inclination in the major part of the slope was also 1/10; the inclination near the side walls, however, was increased to 1/2.8 to generate large lateral flow.

For the improvement piles, aluminium-made pipes were used instead of cement-treated piles so that the piles were fixed to the bottom of the specimen container. In terms of understanding liquefied ground flow interrupted by fixed piles, this modelling was considered simple and uncomplicated. The aluminium pipes have a thickness of 1 mm and an external diameter of 15 mm, corresponding to 0.75 m in a prototype scale. The sand used for the non-liquefiable and liquefiable layers were Iide sand (mean diameter D_{50} = 0.174 mm) and Sohma sand (mean diameter D_{50} = 0.35 mm) mixed with non-plastic silica powder (mean diameter D_{50} = 0.05 mm). The ratio of the dry weights of the Sohma sand and silica powder was 7:3. Sand layers were formed using a sand-raining technique in the air, aiming to reach relative densities of 90% and 50% for the non-liquefiable and liquefiable layers, respectively. Silica powder was mixed to make the liquefiable layer to reduce the permeability of the ground. Viscous fluid is commonly used in a centrifuge to delay the dissipation of excess pore water pressure. Viscous fluid, however, tends to reduce flowability. Takahashi et al. (2014) revealed that the flowability of liquefied ground can be increased by using sand mixed with fine content and water instead of viscous fluid and that a liquefaction-induced landslide can be reproduced. In the present study, the permeability of the ground was also decreased using silica powder, and the dissipation of the excess pore water pressure was delayed. The similitude ratios used in the model tests are summarized in Table 2.

Table 1 Test cases (values are shown in a model scale)

Case	Improvement pattern	Pile diameter, D	Distance between piles	Thickness of ground	Maximum shaking acceleration	Time period of major shaking
UN	Nil	-	-	250 mm	3.4 m/s^2	1 sec
R2d-s I2d-s	Regular Irregular	15 mm	30 mm (2D)	182 – 347 mm	1.6 m/s^2	0.5 sec
R2d-l I2d-l	Regular Irregular	15 mm	30 mm (2D)	182 – 347 mm	3.3 m/s^2	1 sec
R2.5d I2.5d	Regular Irregular	15 mm	38 mm (2.5D)	182 – 347 mm	2.3 m/s^2	0.5 sec
R3d I3d	Regular Irregular	15 mm	45 mm (3D)	182 – 347 mm	2.4 m/s^2	0.5 sec

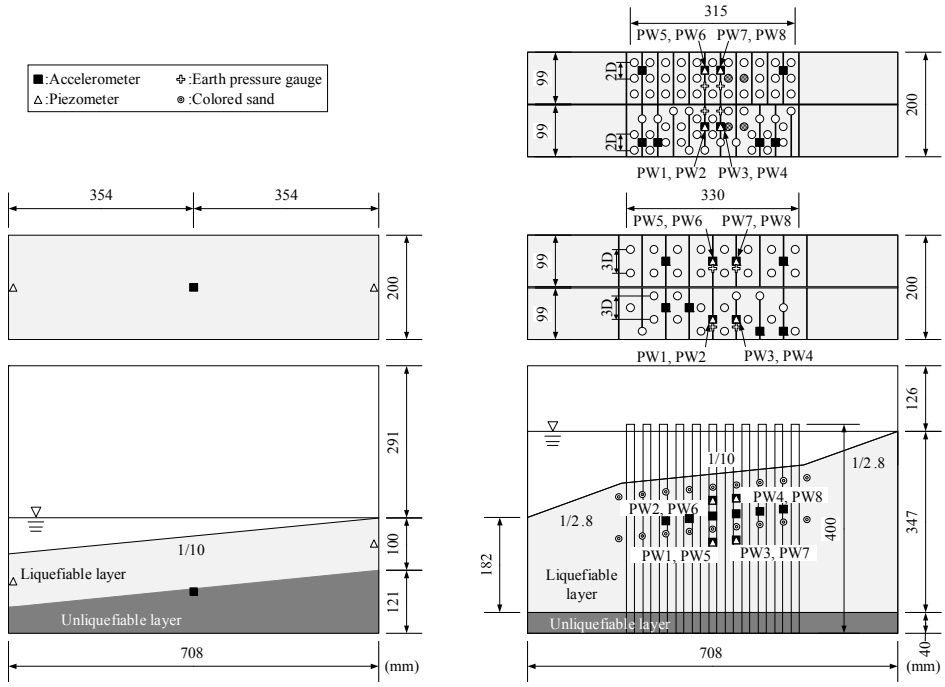

(a) Case UN (b) Cases R2d, L2d, R3d, and L3d

Fig. 3 Vertical cross sections and top views

Table 2 Similitude ratios under centrifuge

Physical parameter	Prototype	Model
Density, ρ	1	1
Stress and pressure, σ, p	1	1
Length, L	1	$1/N$
Time (Dynamic behaviour), t	1	$1/N$
Acceleration, a	1	N
Velocity, U	1	1
Shear strain ratio, $\dot{\gamma}$	1	N
Viscosity coefficient of liquefied soil, μ	1	$1/N$
Viscosity coefficient of water, μ_w	1	1

Test procedure

The prepared test model, a tank accumulating water for pore water, a high-speed camera, and lighting equipment were set on the platform of a centrifuge. The centrifuge used for the tests is owned by the Port and Airport Research Institute, and its effective rotation radius and maximum load capacity are 3.8 m and 2,760 kg, respectively (Kitazume and Miyajima, 1995). After preparing the test model and peripheral device, these were added to a centrifugal acceleration of 30*g*, and water was saturated into the model ground in flight. Okamura and Inoue (2012) reported that the centrifugal acceleration enables rapid percolation for the sake of a large water head and a high saturation degree. The acceleration rose to 50*g*, and the test model was shaken by using a shaking table. Fig. 4 shows the measured input acceleration of two test cases. The frequency of shaking was set to be 100 Hz – corresponding to 2 Hz – in all test cases. Fig. 4(a) of the unimproved case shows that the acceleration was 3.4 m/s^2. Fig. 4(b) represents the acceleration of the improved case, which were 2.4 m/s^2. The test cases, except for Cases R2d-l and I2d-l, had two kinds of magnitude of input acceleration. The latter small acceleration, which were 0.3 – 0.5 m/s^2, was attempted to continue lateral flow for an extended period of time.

Response acceleration and pore water pressure in the ground were gauged during shaking by using miniature sensors. The lateral displacement was measured by coloured sand bars embedded in the ground after the model tests. The lateral displacement was also observed through a window by a high-speed camera attached on the centrifuge platform, and the images were analysed after the model tests. The deformation was determined by the digital image correlation (DIC) technique. DIC is a mathematical tool that assesses spatial transformation between images. The two-dimensional DIC (2D-DIC) analysis code used in this study was developed by referencing Hall et al. (2006). The code follows the same basic steps of most DIC procedures for strain analysis.

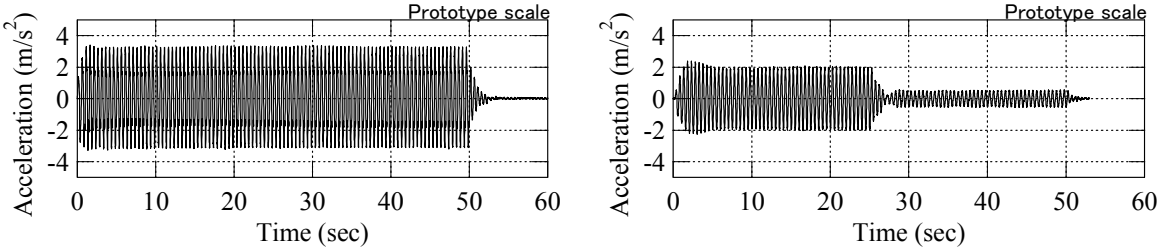

(a) Case UN (b) Cases R3d and I3d

Fig. 4 Input accelerations

Test results of unimproved case

This section discusses the test results of the case where the ground was not improved. First, it needed to be confirmed that the ground fully liquefied due to the increase of pore water pressure during shaking. Fig. 5 represents the time history of the excess pore water pressure ratio, which was measured by the pore water pressure gauge attached on the downstream side wall, in a proto-type scale. The ratio was obtained by dividing the excess pore water pressure by the effective overburden pressure. The effective overburden pressure dramatically changed during shaking due to the slope failure. This is because the value of the downstream sensor is compensated by taking into consideration the change of the effective overburden pressure. As shown in Fig. 5, the ratio at the downstream sensor reached 1.0, and it could be confirmed that the ground fully liquefied.

Fig. 6 shows the distribution of the maximum flow velocities measured in the centre of the ground in a proto-type scale. These velocities were calculated by the DIC method using images from a high-speed camera and obtained by compounding the horizontal and vertical velocities. Although the slope finally broke because of shaking, as described previously, the velocities at an initial stage of shaking before the failure of the slope are shown in the figure. Fig. 5 shows that the ground was fully saturated 4 s after shaking began. In addition, the inclination of the slope was 1/10 – 1/10.5 at this stage, which could almost remain the initial inclination. As shown in the figure, the distribution of the velocity shows that the ground flowed faster in the shallower ground and was similar to that of the viscous fluid. Although the bottom depth of the liquefied layer was 5 m in a prototype scale, the ground at a depth of 4 m and deeper did not significantly flow. This depth was used as a bottom surface in the numerical analysis. The maximum shear strain rate calculated by the velocities was 0.03 – 0.20 1/s in a prototype scale. This value was also used in the numerical analysis.

Fig. 7 shows the time histories of the flow velocity at a depth of 1, 2, 3, and 4 m in a prototype scale. These were also obtained by compounding the horizontal and vertical velocities. As Fig. 5 shows that the ground fully liquefied after 4 s, the ground can be said to be roughly liquefied when the flow velocity reached maximum. According to the figure, the velocity at the depth of 1 m increased to approximately 0.6 m/s initially and thereafter decreased to 0.3 m/s. This is because the dragging force by self-weight

declined owing to the depression of the inclination, and the lateral flow was slowed by the friction force of the bottom surface and the effect of the side walls. In the numerical analysis, in which the depression of the inclination and the effect of the side walls were not taken into consideration, the velocity was simulated until it was maximized.

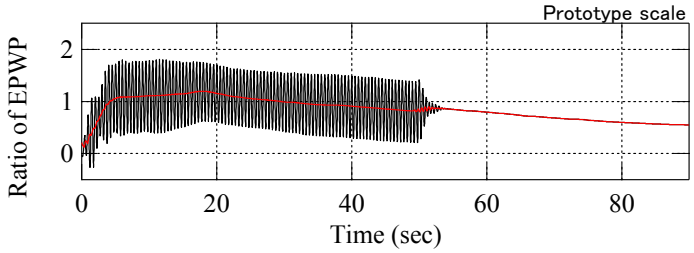

Fig. 5 Time history of excess pore water pressure ratio (Case UN)

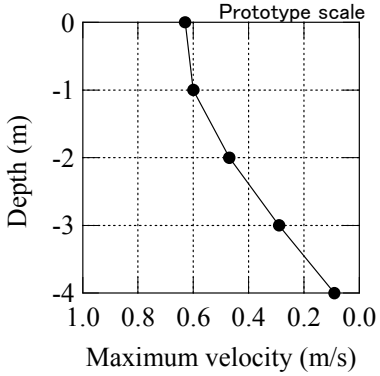

Fig. 6 Distribution of flow velocities

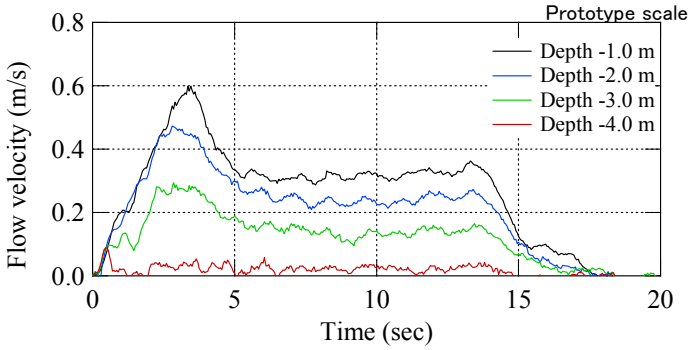

Fig. 7 Time histories of flow velocity

Test results of improved case

This section describes the test results of the case in which the ground was improved by piles. It was confirmed that the excess pore water pressure ratio reached 1.0 due to several seismic motions, and the ground was found to be fully liquefied. As mentioned in the "Prepared model ground" section, coloured sand bars were embedded into the ground, which enabled the observation of the displacement of the ground before and after shaking. Fig. 8 shows the locations of the sand bars after the test. The sand bars were embedded at three depths, and only the displacement at a depth of 1.25 m – corresponding to 25 mm in a model scale – is shown in the figure fore reference. According to the solid lines in the figure, the displacement between piles prone to the flow was found to be small; the displacement between piles perpendicular to the flow was large in contrast. For example, the latter displacements in Cases R2d-l and I2d-l reached 0.95 – 1.10 m and 0.90 – 0.95 m in a prototype scale, respectively.

The displacement at the same depth in the unimproved case reached 6.3 m. The displacements in the unimproved and improved cases cannot be directly compared because their models and the shaking to which they were subjected were different. Compared with these, however, the pile improvement dramatically reduced the displacement, and the reduction ratio was approximately 14 – 17%. The flow velocities between the piles, which were obtained by dividing the displacement by the shaking time, were 19 – 22 mm/s and 18 – 19 mm/s in the regular and irregular cases, respectively. By considering these values to be the velocity at the middle point of the piles, the shear strain rates were 0.048 – 0.059 1/s in a prototype scale.

Fig. 9 shows the average lateral displacements at the centre of the ground in case, which were obtained by dividing the total displacement of a sand bar by its length. Although the plots are scattered, the

displacements in the irregular case were found to be smaller than those in the regular Cases R2d-l and I2d-l. These values were divided by the shaking time to obtain the mean of the average flow velocities; these are summarized in Table 3. The table also includes the maximum and minimum of the average flow velocities. The mean of the average flow velocity decreased in the irregular case or by narrowing the distance between the piles.

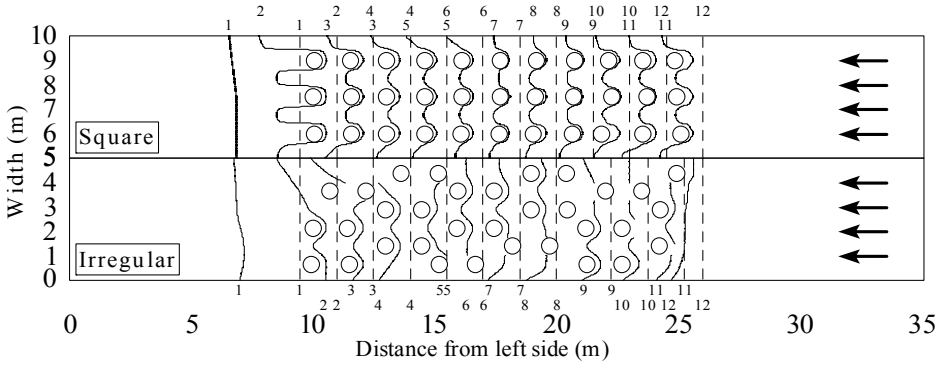

Fig. 8 Locations of coloured sand bars after the tests (Case R2d-l, I2d-l)

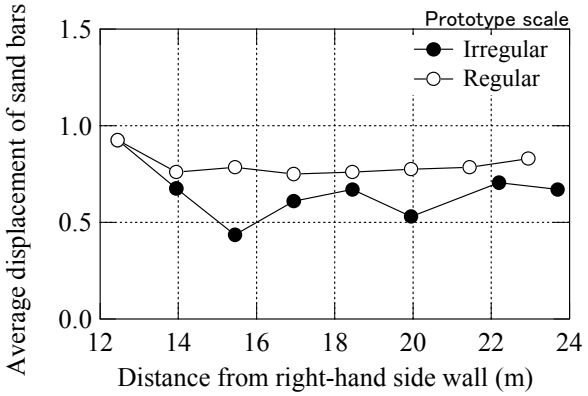

Fig. 9 Displacement of coloured sand bars (Case R2d-l, I2d-l)

Table 3 Average flow velocities

Case	Improvement pattern	Pile diameter, *D*	Distance between piles	Mean velocity	Maximum velocity	Minimum velocity
R2d-s I2d-s	Regular Irregular	15 mm	30 mm (2*D*)	14.5 mm/s 9.4 mm/s	16.4 mm/s 15.7 mm/s	12.4 mm/s 6.2 mm/s
R2d-l I2d-l	Regular Irregular	15 mm	30 mm (2*D*)	15.9 mm/s 13.1 mm/s	18.5 mm/s 18.5 mm/s	15.0 mm/s 8.7 mm/s
R2.5d I2.5d	Regular Irregular	15 mm	38 mm (2.5*D*)	21.8 mm/s 18.0 mm/s	31.6 mm/s 29.2 mm/s	15.7 mm/s 12.8 mm/s
R3d I3d	Regular Irregular	15 mm	45 mm (3*D*)	43.0 mm/s 36.4 mm/s	60.4 mm/s 51.6 mm/s	25.6 mm/s 20.4 mm/s

NUMERICAL FLUID ANALYSES

Concept of numerical fluid analyses

Several techniques have been proposed to simulate the ground deformation of liquefied soil, including (1) the effective stress analysis coupling soil and pore water; and (2) the fluid analysis modelling liquefied soil as a fluid. The former method has been frequently used to determine ground stability and deformation behaviour but has difficulty simulating largely deformed ground. The latter method just models softened soil after liquefaction and is unable to solve such problems as the softening process of liquefiable soil and the sedimentation of liquefied soil. However, the fluid analysis can be used to understand the various flow behaviours of fluid and the mechanism on the effect of the piles because of the simplicity in using limited parameters. Therefore, the fluid analysis was used in the present study.

The behaviour where piles resist the flow of liquefied soil and displacement is reduced is similar to the behaviour in which fluid flows around piles. These problems strongly depend on the Reynolds number. According to this number, the viscosity coefficient and the diameter of a pile are key factors for discussing the flow properties and the effect of the piles. Here, the viscosity coefficient was obtained by reverse analysis to simulate the unimproved case. In previous studies by other researchers, a non-Newtonian model has often been used to model shear strength (e.g., Uzuoka et al., 1998; Hadush et al., 2000; Montassar and Buhan, 2013). However, the present study used a Newtonian model because of its simplicity. This method uses the superficial viscosity coefficient, which could approximately reproduce the shear strength characterizing the flow property in the model.

The calculation was conducted by the COMSOL program (Zimmerman, 2006; Pryor, 2012), which enables the discretization of physical governing equations in three dimensions by using the finite element method. In the analyses, the side walls of the specimen container and the free surface were not modelled, and the flow was simply considered to be a uniform flow with the input and output boundary conditions. Although an inertia force occurred in the model ground due to shaking, this was not taken into account. The present study determined that the time-mean flow velocity was not strongly influenced by alternately repeated forces. The governing equations were the continuity and Navier-Stokes equations

Simulation of unimproved case

The unimproved case was reproduced by an inverse analysis using the fluid analysis to determine the superficial coefficient of viscosity used in the following analyses. The calculation was conducted in a model scale. The thickness of the ground was set to be 80 mm, corresponding to 4 m. This is because the ground in the model test at a depth of 4 m – corresponding to 80 mm – and deeper did not move very much, although the bottom surface was at a depth of 5 m. In the model test, the coloured sand bars moved in a parallel manner, and the influence of the walls could not be observed. Based on this result, the boundary condition between the fluid and wall was set to be free. However, the condition between the fluid and bottom surface was fixed because the flow velocity was almost zero therein. The flow velocity was set to zero as an initial condition. The dragging force to accelerate the ground was 5*g* per unit weight and volume, which corresponded to 0.1 times the centrifugal acceleration of 50*g*. Therefore, the ground was inclined to approximately 1/10. The viscosity coefficient was changed to 200, 500, and 1250 Pa·s, corresponding to 10, 25, and 63 kPa·s in a prototype scale.

Fig. 10 shows the time history of the calculated flow velocity at the ground surface. This figure includes the flow velocity measured in the model test. The velocities of the analysis and the model test are compared until the flow velocity reaches maximum. During the first period, the velocities did not coincide well, probably because the ground in the model was not fully liquefied. However, the velocities with a

viscosity coefficient of 25 kPa･s coincided when the flow was accelerated. Fig. 11 illustrates the flow velocity distribution of the analysis and the model test when the flow velocity in the analysis became constant. This figure shows that the distributions were in agreement when the viscosity coefficient of 25 kPa･s was used. Based on these results, it can be stated that the liquefied ground had a superficial viscosity of 25 kPa･s, corresponding to 500 Pa･s in a model scale.

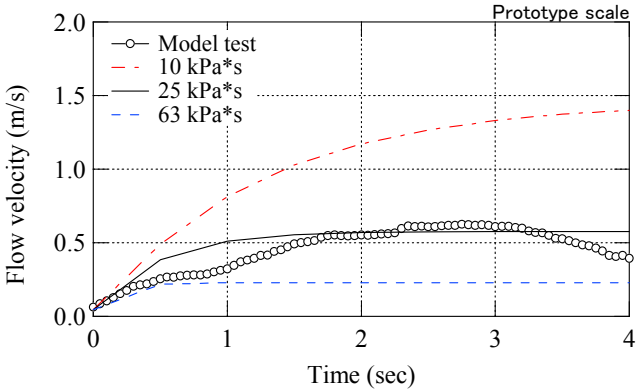

Fig. 10 Time history of flow velocity at ground surface

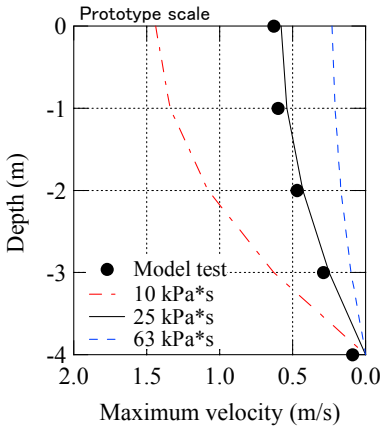

Fig. 11 Distribution of flow velocities

Simulation of improved case

The improved cases using piles were simulated by the fluid analyses. Table 4 shows the list of all analysis cases. These analyses were conducted in a model scale. The bottom surface was set to 260 mm – corresponding to 13 m in a prototype scale – on which the flow velocity was almost zero. The sliding condition on the surface was fixed. The number and arrangement of piles were fitted to those of the model tests. The dragging force was assumed to be 5*g*, which was 0.1 times the centrifuge acceleration of 50*g*. The shear strain rates of the lateral flow in the unimproved case and the flow between the piles in the improved case are not very different, and 500 Pa･s in a model scale was used as the viscosity coefficient without any changes.

Fig. 12 shows the flow velocity distribution at a depth of 1.25 m in a prototype scale of the case with a pile distance of 2*D*. The point at which the velocity was large coincided with the velocity at which the displacement was large in the model test shown in Fig. 8. This result suggests that the analysis could precisely reproduce the test. In addition, the flow velocities between the piles around the centre of the ground were 19 and 19 – 28 mm/s; these are 3.5 – 4.4% of the velocity of the unimproved case. The velocities were similar to those in the model tests. Table 5 summarizes the average flow velocity of each analysis case at a depth of 1.25 m, corresponding to 25 mm in a model scale. Compared with the velocities listed in Table 3, the velocities of the model tests and analyses were almost similar. Changing the pile arrangement from regular to irregular could roughly reduce the velocity.

Finally, the effect of the pile arrangement is discussed. The piles prevent the fluid flow and the velocity around the piles increases. It is well-known that the area with a high velocity extends toward the downstream side. When the pile arrangement is irregular, the high-velocity area comes up against the downstream pile, and the velocity can be reduced. However, the high-velocity areas overlap and the velocity between the piles increases when the pile arrangement is regular. This difference between flows is believed to cause the contrast between the regular and irregular arrangements.

Table 4 Analysis case and conditions (values are shown in a model scale)

Case	Improvement pattern	Pile diameter, *D*	Distance between piles	Thickness of ground	Dragging force	Viscosity coefficient
S-R2d S-I2d	Regular Irregular	15 mm	30 mm (2*D*)	182 – 347 mm	5*g*	8 & 500 Pa·s
S-R2.5d S-I2.5d	Regular Irregular	15 mm	38 mm (2.5*D*)	182 – 347 mm	5*g*	500 Pa·s
S-R3d S-I3d	Regular Irregular	15 mm	45 mm (3*D*)	182 – 347 mm	5*g*	500 Pa·s

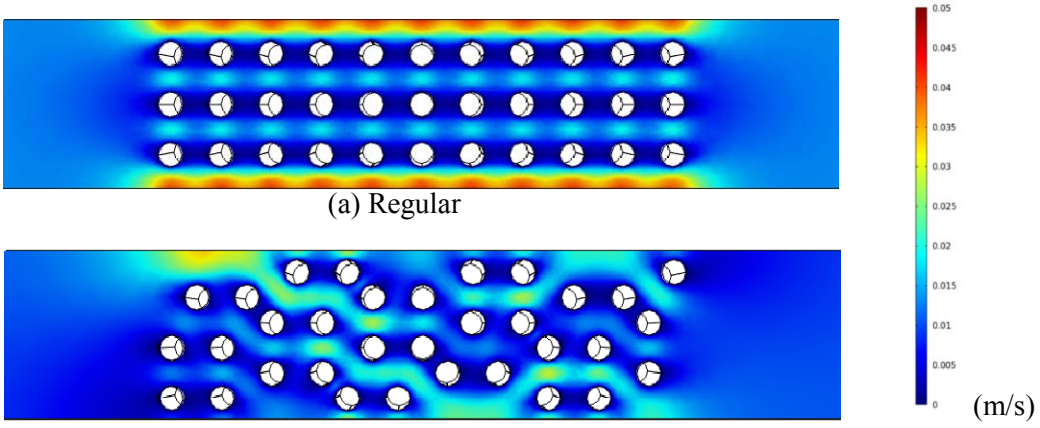

(a) Regular

(b) Irregular

Fig. 12 Flow velocity distribution calculated by numerical analysis

Table 5 Average total flow velocities in numerical analyses

Case	Improvement pattern	Pile diameter, *D*	Distance between piles	Mean velocity
S-R2d S-I2d	Regular Irregular	15 mm	30 mm (2*D*)	14.1 mm/s 10.4 mm/s
S-R2.5d S-I2.5d	Regular Irregular	15 mm	38 mm (2.5*D*)	19.5 mm/s 20.4 mm/s
S-R3d S-I3d	Regular Irregular	15 mm	45 mm (3*D*)	51.9 mm/s 43.4 mm/s

CONCLUSIONS

In the present study, a series of centrifuge model tests were implemented to clarify the efficacy of the pile improvement and the influence of the piles' arrangement. In ground flow, model piles were arranged in two patterns: regular and irregular. Then, numerical fluid analyses were conducted to consider the improvement mechanism and the cause generating the difference in the two patterns of arrangement. As a result, the model tests and numerical analyses showed that the pile improvement dramatically reduced the lateral displacement and that the average total flow velocity decreased in the irregular case.

REFERENCES

Hadush, S., Yashima, A., and Uzuoka, R. 2000. Importance of viscous fluid characteristics in liquefaction induced lateral spreading analysis, Computers and Geotechnics, Vol. 27, pp. 199-224.

Hall, S.A. 2006. A methodology for 7D warping and deformation monitoring using time-lapse seismic data, Geophysics, Vol. 71, No. 4, pp. O21-O31.

Hamada, M., Isoyama, R., and Wakamatsu, K. 1996. Liquefaction-induced ground displacement and its related damage to lifeline facilities, Soils and Foundations, Vol. 36, Special Issue, pp. 81-97.

Hamada, M. and Wakamatsu, K. 1998. A study on ground displacement caused by soil liquefaction, Journal of Japan Society of Civil Engineers, No. 596 / III-43, pp. 189-208. (in Japanese)

Kitazume, M. and Miyajima, S. 1995. Development of PHRI Mark II geotechnical centrifuge, Technical Note of the Port and Harbour Research Institute, No. 812, 35 p.

Morikawa, Y., Takahashi, N., Tsuda, W., Towhata, I., Takahashi, H., Sassa, S., and Kohama, E. 2014. Dynamic centrifuge test on the reduction of lateral flow of liquefied ground by column type stabilization, Proceedings of International Conference on Piling & Deep Foundations, Stockholm, pp. 703-712.

Montassar, S. and Buhan, P.D. 2013. Numerical prediction of liquefied ground characteristics from back-analysis of lateral spreading centrifuge experiments, Computers and Geotechnics, Vol. 52, pp. 7-15.

Nishimura, S., Towhata, I., and Honda, T. 2002. Laboratory shear tests on viscous nature of liquefied sand, Soils and Foundations, Vol. 42, No. 4, pp. 89-98.

Okamura, M. and Inoue T. 2012. Preparation of fully saturated models for liquefaction study, International Journal of Physical Modelling in Geotechnics, Vol. 12, Issue 1, pp. 39-46.

Pryor, R.W. 2012. Multiphysics Modeling Using COMSOL 4: A First Principle Approach, Mercury Learning & Information, 700p.

Takahashi, H., Sassa, S., and Morikawa, Y. 2014. Centrifuge modelling of earthquake-induced submarine landslide and its gravity flow transition, Proceedings of the 8th International Conference on Physical Modelling in Geotechnics, Perth, pp. 1009-1015.

Takahashi, N., Derakhshani, A., Rasouli, R., Towhata, I., and Yamada, S. 2013. Shaking model tests on mitigation of liquefaction-induced ground flow by new configuration of embedded columns, Proceedings of the 18th International Conference on Soil Mechanics and Geotechnical Engineering, Paris, pp. 1623-1626.

Uzuoka, R., Yashima, A., Kawakami, T., and Konrad, J.M. 1998. Fluid dynamics based prediction of liquefaction induced lateral spreading, Computers and Geotechnics, Vol. 22, pp. 242-282.

Zimmerman, W.B.J. 2006. Multiphysics modeling with finite element methods, World Scientific, 432p.

DYNAMIC CENTRIFUGE MODEL TESTS ON PILE-TYPE DEEP MIXING METHOD REDUCING LATERAL FLOW OF LIQUEFIED GROUND

Yoshiyuki Morikawa, Port and Airport Research Institute, Yokosuka, Japan, morikawa@pari.go.jp
Hidenori Takahashi, Port and Airport Research Institute, Yokosuka, Japan, takahashi-h@pari.go.jp
Tsuda Wakaki, Sumitomo-Mitsui Construction Co., Nagareyama, Japan, WakakiTsuda@smcon.co.jp
Natsuki Okuno, Sumitomo-Mitsui Construction Co., Nagareyama, Japan, n_okuno19@smcon.co.jp
Naoki Takahashi, Sumitomo-Mitsui Construction Co., Nagareyama, Japan, tnaoki@smcon.co.jp
Ikuo Towhata, University of Tokyo, Tokyo, Japan, towhata@geot.t.u-tokyo.ac.jp

ABSTRACT

Deep mixing (DM) method has been increasingly employed as a countermeasure against subsoil liquefaction in recent years. Pile-type DM, however, is considered to have little effect as a liquefaction countermeasure, because the shear deformation of unimproved soil around the piles cannot be reduced. However, experimental results, which imply that shear deformation of unimproved soil around DM piles can be reduced, were reported. Furthermore, a new plane-arrangement of DM piles has been proposed to mitigate lateral flow induced by liquefaction. The DM piles in this arrangement confront the lateral flow in any direction, compared with the piles arranged in conventional pattern such as square and triangular arrangements. In this study, a series of dynamic centrifuge model tests was conducted to verify the lateral flow resistance of DM plies in the new arrangement. The results indicate that the DM plies can reduce the lateral flow of liquefied ground when the pile displacement and the pile head rotation are restricted. In addition, lateral load acting on DM pile from liquefied ground, which is required for design strength of the DM pile, was investigated.

Keywords: deep mixing pile, liquefaction, lateral flow, plan arrangement

INTRODUCTION

Deep mixing (DM) method has been increasingly employed as a countermeasure against subsoil liquefaction in recent years. The solidified body formed by the deep mixing method is usually block or lattice shape, composed of solidified columns that overlap each other horizontally. Lattice-type solidification has been shown to be effective as a liquefaction countermeasure despite the presence of unimproved soil inside the lattice wall, because the shear deformation of the interior soil is restrained by the wall (Suzuki et al., 1989). On the other hand, it has been thought that pile-type DM cannot reduce shear deformation of unimproved soil around the piles, because the displacement of the pile is less restricted than that of the lattice wall. DM piles has been reported to have little effect as a liquefaction countermeasure, but to be superior in terms of construction cost and applicability around existing underground structures (Koga et al., 1986). However, there are experimental results implying that DM piles have reduced the shear deformation of unimproved soil and mitigated its liquefaction (Yasuda et al., 2003; Tanaka et al., 2003). Yamamoto et al. (2006) conducted dynamic analyses of ground improved with lattice- and pile-type DM. Their results showed that pile-type DM with an improvement ratio of more than 35% reduces excess pore water pressure generated by earthquakes. Furthermore, the new pile arrangement shown in Fig. 1(a) has been proposed to mitigate lateral flow induced by liquefaction. It was developed and has been verified using dynamic model testing in a 1 g field (Takahashi et al., 2010a; 2010b; 2013; Towhata et al., 2010, Morikawa et al., 2014). The DM piles in this configuration interrupt lateral flow in any direction, unlike those placed in square and triangular arrangements.

In order to raise the resistance of the DM piles to lateral flow, pile-type DM should be used together with surface improvement. Surface improvement restricts the relative displacement between the DM piles and the pile head rotation. In this study, a series of dynamic centrifuge model tests was conducted to verify the

lateral flow resistance of the DM piles whose heads are fixed by surface improvement. This paper concludes that it is important to secure the rigidity between the pile head and the surface improvement to mitigate lateral flow of liquefied ground. In addition, it is shown that the lateral load acting on the pile from liquefied ground, which is required for design strength of the DM pile, can be estimated by the method in "Specifications for Highway Bridges" (Japan Road Association, 2002).

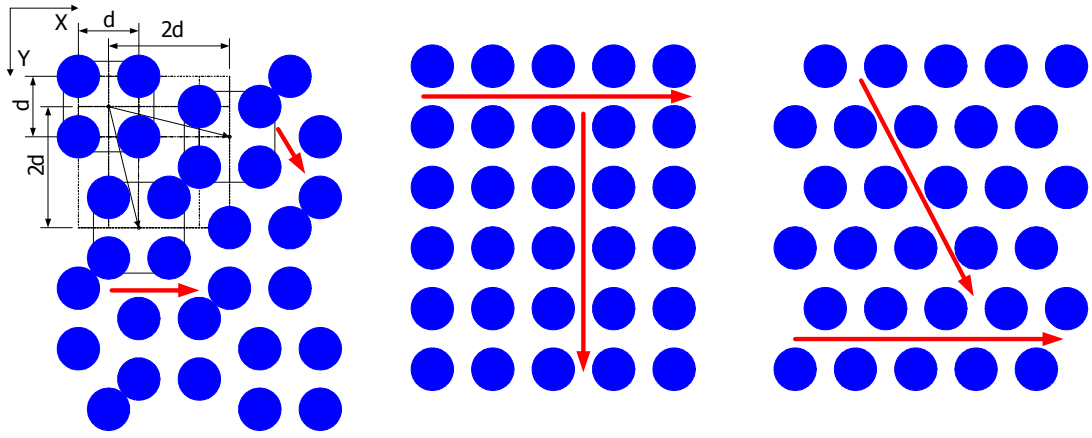

(a) New arrangement (b) Square grid pattern (c) Triangular grid pattern

Fig. 1. Arrangement of DM piles

TEST CONDITIONS AND PREPARATION

Test Apparatus

The centrifuge facility owned by the Port and Airport Research Institute was used for model test. It has a radius of 3.8 m, a maximum payload of 2.7 metric tons and a maximum acceleration of 113 g. The details of the centrifuge can be seen in the report by Kitazume and Miyajima (1995). In this study, dynamic model tests were carried out in a centrifugal acceleration field of 50 g. Table 1 shows the scaling laws for modeling a subject to a centrifugal acceleration of n × g.

Table 1. Centrifuge scaling laws

Parameter	Model/Prototype	Dimensions
Length	$1/n$	L
Acceleration	n	LT^{-2}
Displacement	$1/n$	L
Strain	1	1
Stress	1	$ML^{-1}T^{-2}$
Force	$1/n^2$	MLT^{-2}
Time (seepage)	$1/n^2$	T
Time (Dynamic)	$1/n$	T

A viscous aqueous solution of cellulose ethers (Brand name: METOLOSE) was used to saturate the model ground. The kinematic viscosity of the solution was set to 50 cSt to fit the scaling laws for both dynamic and seepage phenomena in a centrifugal acceleration field of 50 g.

A rigid box was used as specimen container and it had the following inner dimensions: width = 200 mm, height = 512 mm, and length = 708 mm. The back, bottom, and both side walls of the container were made of aluminum plate. The front side wall was an aluminum frame with a viewing window of tempered glass for observation of ground behavior.

Test Conditions

A schematic diagram of the model ground is shown in Fig. 2. A 1:n model experiences the same stress-strain conditions as a prototype in a centrifugal acceleration field of $n \times$ g (Schofield 1980, 1981). The model ground was composed of two sand layers made of Sohma sand #5 (G_s = 2.65, e_{min} = 0.71, e_{max} = 1.115). The lower was a non-liquefiable base layer 40 mm thick and with 90% of relative density. The upper layer was a liquefiable layer at 40% relative density. Its surface was inclined at 10% to induce lateral flow. In this study, six model tests were conducted, including one with unimproved ground, with different arrangements of DM piles and geometric boundary conditions at the pile heads. In the cases where the ground was improved, twelve acrylic pipes, with 40 mm outer diameters (corresponding to 2 m on the prototype scale), were used as DM piles with a common improvement ratio of 35 %. Acrylic was used in order to avoid unnecessary complications caused by yielding or bending failure of the pile.

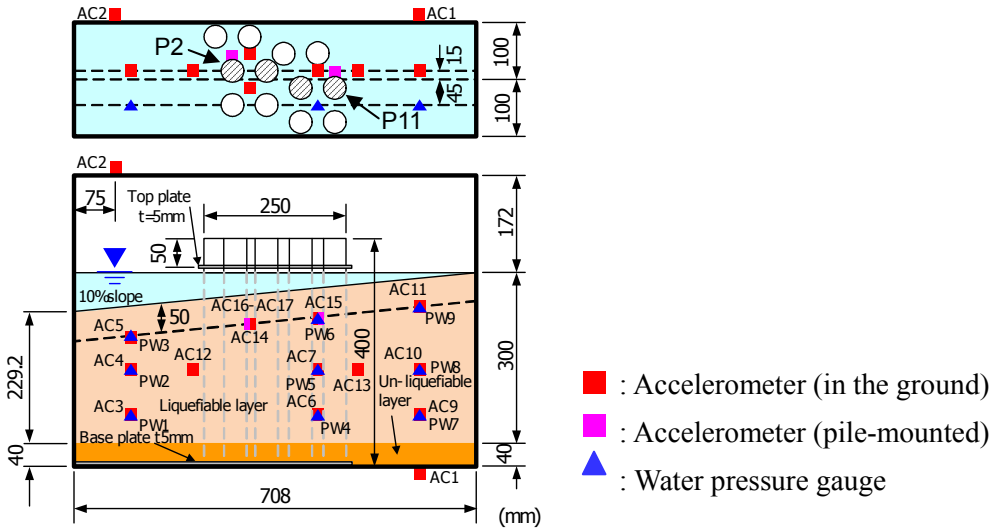

Fig. 2. Schematic view of model ground

The test conditions for each case are shown in Table 2. In the table, the new arrangement of piles to be verified in this study is designated as “irregular” for convenience, though it is regular in some respects. In Cases 2 to 5, a base plate, made of thin (5 mm) acrylic material, was placed on the bottom of the container. The base plate had holes with diameters (44 mm) slightly larger than the diameter of the piles, cut at the pile position. The remaining space between the plate and piles allowed free rotation and minor lateral displacement of the pile toe. In Cases 2 and 5, other than Case 3, pile displacement was restricted by an identical plate. Thus, in those cases, there was hardly any relative displacement among the pile heads, but they could rotate. In Case 4, the acrylic plate and pile heads were rigidly connected. Consequently, neither rotation nor relative displacement was permitted at the pile heads.

Table 2. Test conditions

Test case	Arrangement of piles	Improvement ratio (%)	Geometric boundary condition at pile head
Case 1	-	0	-
Case 2	irregular	35	pin joint
Case 3	irregular	35	free
Case 4	irregular	35	fixed by plate
Case 5	regular (square grid pattern)	35	pin joint

The arrangements of the piles used in this series of tests are shown in Fig. 3. Some piles that did not lie within the specified improvement area (drawn by dashed lines in Fig. 3) were not put in place in order to avoid complications. Consequently, the same number of piles was placed in both arrangements.

In the dynamic model tests, 50 sinusoidal waves with a frequency of 100 Hz (corresponding to 2 Hz on the prototype scale) were applied in a centrifugal acceleration field of 50 g. The amplitude of the input waves was 100 Gal (corresponding to 200 Gal on the prototype scale).

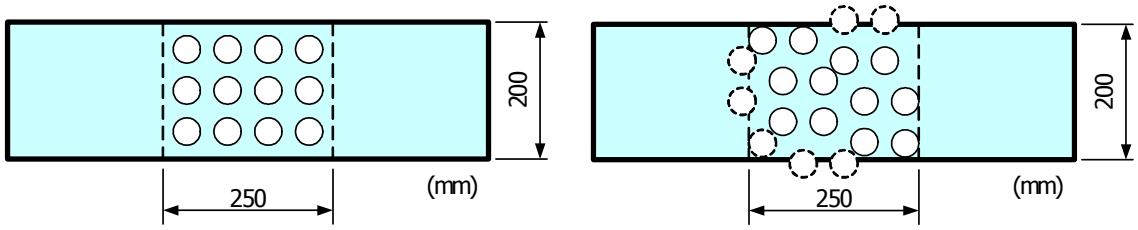

(a) Regular pattern (square grid pattern) (b) Irregular pattern

Fig. 3. Arrangement of piles in dynamic centrifuge tests

Measurement

Figure 2 also shows the location of sensors placed for measurement. During vibration, the acceleration and pore water pressure in the model ground were recorded, in addition to the acceleration of two piles. Strain gauges were arranged in a line and glued onto the periphery of the piles shown crosshatched in Fig. 2. The gauges were glued on the upstream and downstream sides of the piles in order to obtain the bending moment. This bending moment was used for estimation of lateral flow pressure acting on the pile from liquefied ground. Lines of colored sand, made of the same material as the model ground, were formed on the front side and surface of the model ground. This was used to trace the distribution of lateral displacement in the vertical and horizontal directions.

Model Ground Preparation

In this study, the DM piles were simulated by acrylic pipes as described earlier. Their outer diameter was 40 mm and their inner diameter was 28 mm. The weight of the pipes was adjusted to satisfy the centrifuge scaling law by installing steel rods on their interior and filling the remaining space with silicone.

To prepare the model ground, the base plate was first placed at the designated position at the bottom of container. Then, pipes were set inside the holes in the base plate so that the center of the pipes coincided with those of the holes. The remaining space between the pipes and the holes was filled with silicone grease in order to prevent the sand used to simulate the model ground from clogging. Before preparing the sand layers, sensors were placed at designed heights from the bottom of container with the help of fine fishing lines, which were cut after the container had been filled with sand. The model ground was placed by air pluviation of the sand from a hopper, which was placed high enough so that the ground density would not be influenced by changing drop heights as the sand filled the container. The density of each sand layer was managed by controlling the sand flow rate (Takahashi et al., 2010). The ground surface was carefully smoothed using a vacuum device after pluviation was completed.

After pluviation, the centrifuge was started. Centrifugal acceleration was raised up to 30 g and kept constant. Then, the model ground was gradually saturated by allowing the viscous fluid to infiltrate from the bottom of container until it reached the top of the model ground. Infiltration was induced by keeping the fluid supply bucket higher than the fluid level in the model ground. This infiltration method, assisted

by centrifugal acceleration, was proposed by Okamura and Inoue (2012). Figure 4 shows the completed model grounds of Case 2 as examples.

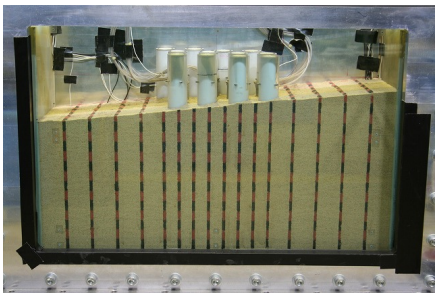

Fig. 4. Examples of completed model ground (Case 2)

DYNAMIC TEST

After infiltration, the centrifugal acceleration was raised again up to 50 g, and dynamic test was conducted. In the dynamic model tests, 50 sinusoidal waves with a frequency of 2 Hz and amplitude of 200Gal on the prototype scale were applied in a centrifugal acceleration field of 50 g, as mentioned above.

Excess Pore Water Pressure

The time histories of excess pore water pressure ratio for Cases 1, 2 and 5 are shown in Fig. 5. The ratio is the excess pore water pressure normalized by the effective overburden pressure at the measuring depth. The time histories in these figures were measured at the middle height of the ground on the upstream side of the improved area (PW5 in Fig. 2). The overburden pressure used to calculate the ratio should be corrected depending on the position of the gauge which changes due to liquefaction and lateral flow. However, the overburden pressure was not corrected because it was difficult to trace the gauges. It is thought that the pore water pressure ratio being more than 1.0 and the residual pressure remaining for a long time after vibration were caused by this problem.

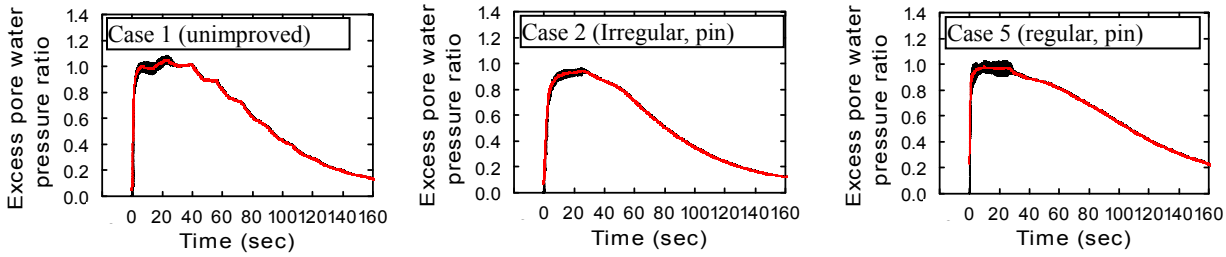

(a) Case 1 (b) Case 2 (c) Case 5

Fig. 5. Time histories of excess pore pressure ratio

Simple moving averages of these time histories, within the wavelength of the input acceleration, are also shown to aid in observing trends in the data without sharp fluctuations during vibration. The pore water pressure ratios increased drastically just after the vibration started and reached almost 1.0. In Cases 3 and 4, behavior of pore water pressure same as Fig. 5 was observed.

Deformation of Model Ground

Figure 6 shows the deformation of the model ground drawn by tracing the colored sand after vibration. In Case 1, the lateral displacement was a maximum at the ground surface while no displacement was

observed at the bottom. Subsidence and uplift were observed on the upstream and downstream sides of the lateral flow, respectively, and the ground surface became almost level. In all cases where the ground was improved by piles, the surfaces of the unimproved ground on the upstream and downstream sides were also leveled, as similar to Case 1. However, the surface gradient of the improved area hardly changed in these cases.

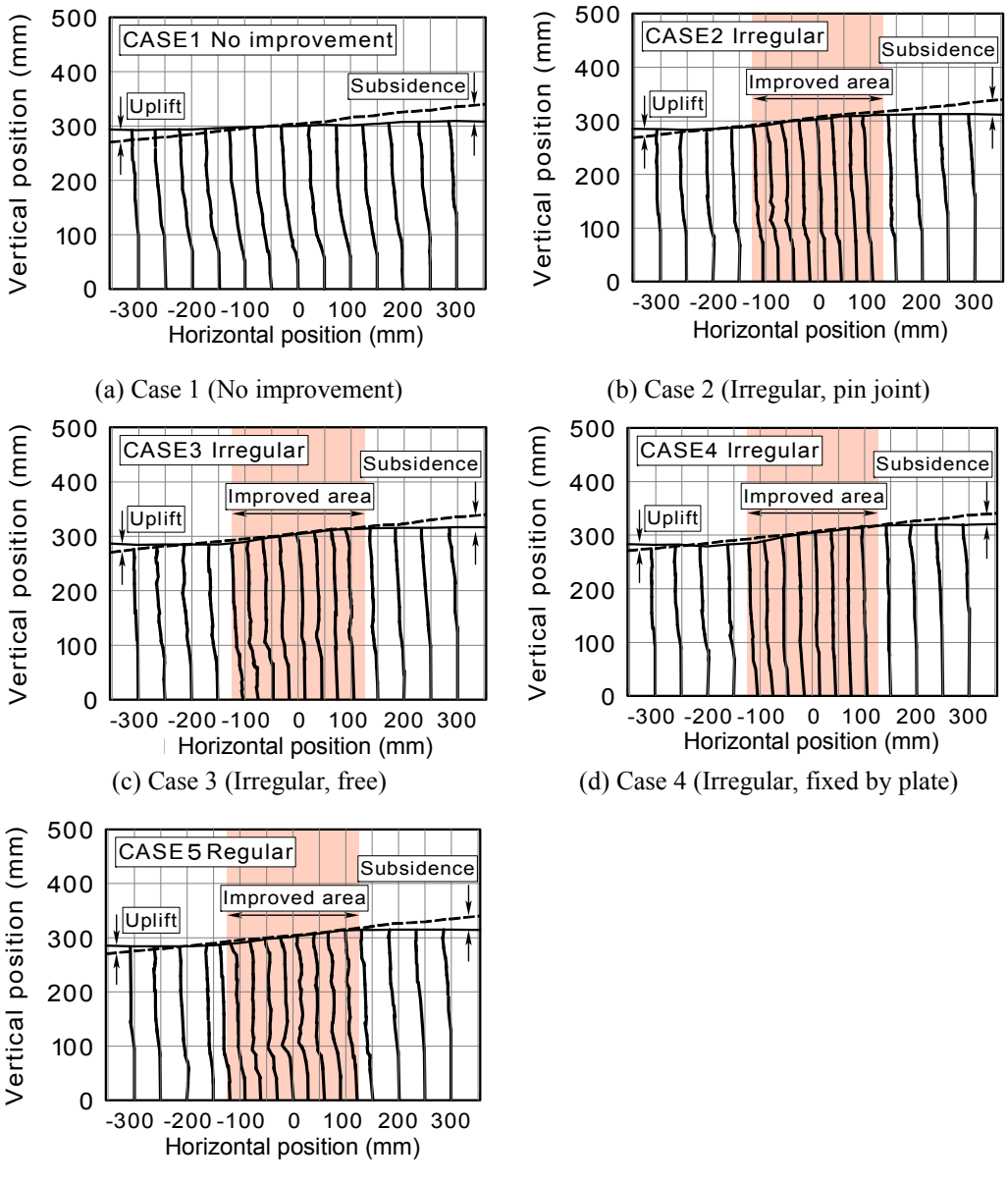

(a) Case 1 (No improvement)

(b) Case 2 (Irregular, pin joint)

(c) Case 3 (Irregular, free)

(d) Case 4 (Irregular, fixed by plate)

(e) Case 5 (Regular, pin joint)

Fig. 6. Deformation of model ground

In Cases 2 to 4, which were improved using piles in the irregular arrangement, the lateral displacement within the improved ground shows a linear distribution in the vertical direction. On the other hand, the lateral displacement fluctuated in the deeper part of the improved area in Case 5, which featured regularly arranged piles. This fluctuation was caused by lateral flow through the improved area because there were continuous gaps between piles connecting the unimproved areas on both sides near the front window. There is no significant difference between the lateral displacement in Cases 2 and 3, though the movement

of pile head was not restricted in Case 3. In observations after Case 3, the piles were found not to be disarranged as has been expected. This small difference between these cases is still debatable, though the difference may be made clear by applying longer or 2-dimensional vibrations. The lateral displacement in Cases 2 and 3 was slightly larger than in Cases 4. This implies that restricting the pile heads is effective at increasing the resistance of the irregularly arranged piles to lateral flow.

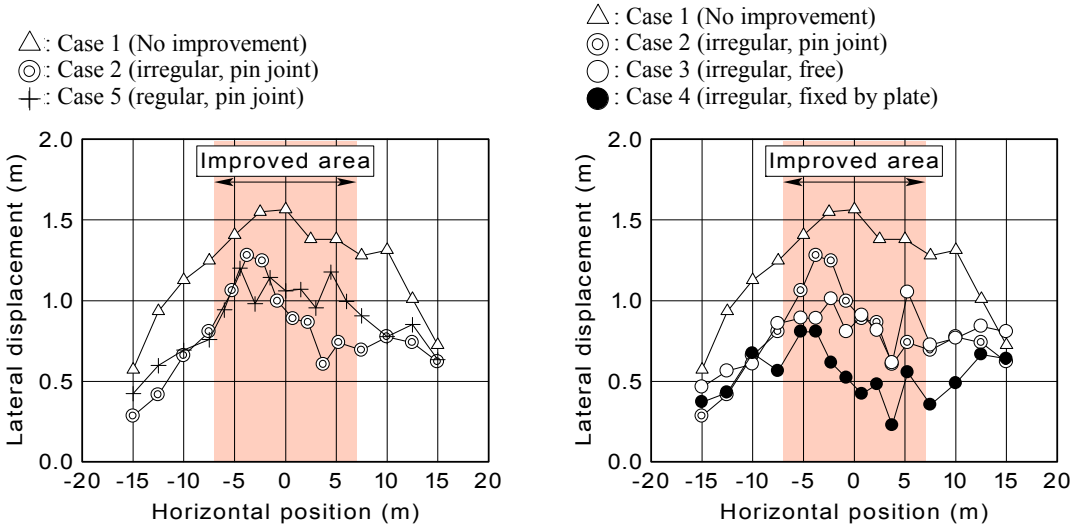

(a) Effect of pile arrangement (b) Effect of restricting pile heads

Fig. 7. Lateral displacement at ground surface after vibration

The horizontal distributions of lateral displacement at the ground surface are shown on the prototype scale in Fig. 7. The displacement was evaluated by observing the colored sand after vibration. The lateral displacement at the ground surface in Case 1 was the largest of all cases over the entire length of the model. It showed a maximum in the middle part of the model. A similar lateral displacement distribution was also observed in a 1-g model test (Sasaki et al., 1992; Takahashi et al., 2013).

Figure 7(a) compares the reduction of lateral displacement for the different pile arrangements. In both Case 2 and Case 5, where the relative displacement and rotation of the pile heads were subjected to the same restrictions, lateral displacement was reduced. However, upstream of the improved area (at horizontal positions from 0 to 10 m), the lateral displacement was smaller in Case 2 than in Case 5. In contrast, at horizontal positions between -5 and -2 m, the displacement in Case 2 was larger than in Case 5. It could be that this large displacement was caused by continuous gaps between piles next to the unimproved area on the downstream side in the model ground used for this series of tests (Fig. 3(b)).

The effect of restriction at the pile heads on reducing the lateral displacement is shown in Fig. 7(b). The reduction in Case 4 was larger than in Cases 2 and 3, similar to the depiction in Fig. 6. In Case 4, the lateral displacement was less than 50% of the displacement in Case 1. These results show that irregular arrangements of piles can reduce the lateral flow of liquefied ground, and that even more reduction can be achieved by restricting the pile heads with work such as surface improvement.

Bending moment of DM piles and pressure induced by lateral flow of liquefied ground

Changes in distribution of bending moment distribution of pile-P11 (in Fig. 2) in Cases 2 and 4 are shown in Fig. 8. The approximation was made using the cubic spline function in drawing the distribution. The approximation curve did not have to coincide with the scattered data plot because the test results will

inevitably contain some errors. Therefore, the smoothing spline function was used for approximation. The moment in bending mode, in which the pile becomes convex to its upstream side, is defined as positive.

In Case 2, the bending moment at the pile head was almost 0 and the pile was bent at the part immediately above the non-liquefiable base layer. Distribution of the bending moment in Case 2 hardly varied during the latter half of the vibration. This means that the pile in Case 2 faced the lateral flow as a cantilever. On the other hand, in Case 4, negative bending moment, which means that the downstream side of the pile was convex, was observed in upper part of the pile due to the restriction at pile head. And the bending moment observed at the part immediately above the non-liquefiable base layer was similar to that in Case 2. It can be said, therefore, that the pile in Case 4 resisted the lateral flow by rigidity at the pile head and toe. In Fig. 8 (c), the bending moment of lower part of the pile decreased to 0, though the moment at the pile head slightly changed. It is found that the restriction by embedment to the non-liquefiable base layer was lost during the latter half of the vibration.

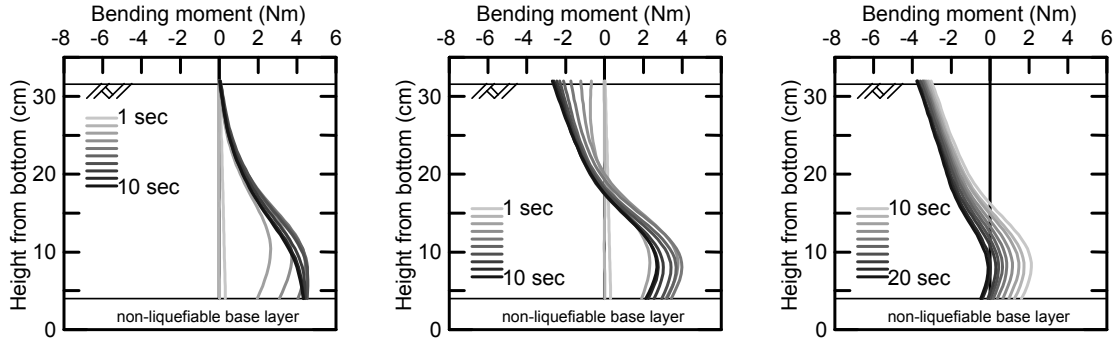

(a) Case 2 (b) Case 4 (0-10 sec) (c) Case 4 (10-20 sec)

Fig. 8. Change of bending moment distribution during vibration

Distributions of lateral load acting on the pile can be obtained by differentiating the spline curve of the bending moment twice. In this study, however, the distribution of the shear force was also evaluated by the cubic spline function before it was differentiated to calculate the lateral load (Kikuchi, 2003). This calculation was conducted to maintain the degree of the spline function. Figure 9 shows the lateral load distributions acting on the piles-P2 and P11 induced by the lateral flow of liquefied ground. These distributions were evaluated from the bending moment distributions at which the maximum bending moment was generated. The lateral load from upstream side was defined as positive.

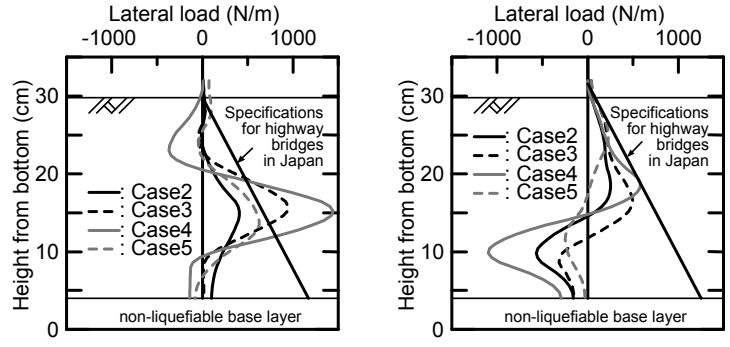

(a) Pile-P2 (b) Pile-P11

Fig. 9. Lateral load distributions acting on the piles from liquefied ground

In all cases, the lateral load distributions have same tendency. The lateral load acting on the upper part of the pile-P11 gradually increases with respect to depth. Furthermore, it is found that the lateral load distributions of the upper part of the pile are approximate to a linear distribution estimated by the method

in “Specifications for Highway Bridges” (Japan Road Association, 2002). However, in lower part of the pile-P11, lateral load from the downstream side was observed. It is thought that this lateral load from the downstream side was caused by small lateral displacement of deeper part of the model ground, which is 0 to 10 cm from the bottom of container, as shown in Fig. 6. The lateral load from upstream side may be generated in deeper part of liquefiable layer in the case of inclined non-liquefiable base layer, though the base layer is horizontal in this study. Therefore, in the design of strength of DM pile, the linear distribution of the lateral load from the liquefied ground calculated by “Specifications for Highway Bridges” can be employed for safety design. On the other hand, large lateral load acted on the middle part of pile-P2 from the upstream side, and it was larger than estimated load by “Specifications for Highway Bridges”. This large lateral load was caused by large lateral displacement of the ground around pile-P2, because pile-P2 was located at the downstream end. However, in the cases of irregular pile arrangement, the large lateral displacement was observed only around the downstream end, as shown in Fig. 7. It can be thought that the lateral load on the second or third pile from the downstream end is smaller than that shown in Fig. 9 (a). Therefore, the lateral load on piles at downstream side can also be estimated to have linear distribution by “Specifications for Highway Bridges”, if there are one or two extra piles at the downstream end, which is small part in whole improved area in practice.

CONCLUSIONS

In this study, a series of dynamic centrifuge model tests was conducted to verify the lateral flow resistance of DM piles in an irregular arrangement and to investigate the lateral load acting on DM pile from liquefied ground, which is required for design strength of the DM pile.

The tests confirmed that DM piles in an irregular arrangement are effective in preventing the lateral flow of liquefied ground. Furthermore, it was found that restricting the displacement between the DM piles and the rotation of the pile heads can further reduce the lateral flow. Therefore, pile-type DM is recommended to be used together with surface improvement.

Based on the bending moment of the pile, in the design of strength of DM pile, it is concluded that the linear distribution of the lateral load from the liquefied ground calculated by “Specifications for Highway Bridges” can be employed for safety design.

REFERENCES

Japan Road Association, 2002. Specifications for highway bridges, Part 5 Seismic design, pp. 130-131 (in Japanese).

Kikuchi, Y., 2003. Lateral resistance of soft landing moundless structure with piles, Technical Note of the Port and Harbour Research Institute, Port and Harbour Research Institute, No. 1039, 192p. (in Japanese).

Kitazume, M. and Miyajima, S., 1995. Development of PHRI Mark II geotechnical centrifuge. Technical Note of Port and Harbour Research Institute, Port and Harbour Research Institute, No. 817, 33p.

Koga, Y., Taniguchi, E., Nakasumi, I. and Awanami, K., 1986. Shaking table tests on deep mixing method against liquefaction of sand deposit. Proceedings of the 41th Annual Conferenfe the Japan Society of Civil Engineering, III, pp. 201-202. (In Japanese)

Morikawa, Y., Takahashi, N., Tsuda, W., Towhata, I., Takahashi, H., Sassa, S. and Kohama, E., 2014. Centrifuge test on reduction of lateral flow of liquefied ground by stabilized columns. Proceedings of International Conference on Piling & Deep Foundations, pp.703-712.

Okamura, M. and Inoue, T., 2012. Preparation of fully saturated models for liquefaction study. International Journal of Physical Modelling in Geotechnics, Vol. 12, No. 1, pp. 39-46.

Sasaki, Y., Towhata, I., Tokida, K., Yamada, K. Matsumoto, H., Tamari, Y. and Saya, S., 1992. Mechanism of Permanent Displacement of Ground Caused by Seismic Liquefaction. Soils and Foundations, Vo. 32, No. 3, pp. 79-96.

Suzuki, Y., Tokito, K., Suzuki, Y. and Babasaki, R., 1989. Introduction examples of soil improvement method by stabilization. The Foundation Engineering and equipment, Vol. 17, No. 9, pp. 87-95. (In Japanese)

Takahashi, H., Morikawa, Y. and Ichikawa, E., 2010a. Effects of rigid sidewall of specimen container on seismic behavior. Proceedings of 7th International Conference on Physical Modeling in Geotechnics, pp. 177-182.

Takahashi, N., Bahmanpour, A., Towhata, I., Yamada, S. and Yamamoto, Y., 2010b. Shaking model tests on column type deep mixing method on liquefaction prevention. Proceedings of the 45th Japan National Conference on Geotechnical Engineering, pp. 1439-1440. (In Japanese)

Takahashi, N., Bahmanpour, A., Towhata, I., Yamada, S. and Yamamoto, Y., 2010. Effective configuration of columns for deep mixing method against lateral flow by liquefaction. Proceedings of the 65th Annual Conference of the Japan Society of Civil Engineering, I, pp. 107-108. (In Japanese)

Takahashi, N., Derakhshani, A., Rasouli, R., Towhata, I. and Yamada, S., 2013. Shaking model tests on mitigation of liquefaction-induced ground flow by new configuration of embedded columns. Proceedings of the 18th International Conference on Soil Mechanics and Geotechnical Engineering, pp. 1623-1626.

Tanaka, T., Yasuda, S., Murasawa, Y., Konishi, T., and Uchiyama, J., 2003. Effects of Column type deep mixing method on liquefaction prevention, Proceedings of the JSCE Earthquake Engineering Symposium, Vol. 27, No. 210. (In Japanese)

Towhata, I., Takahashi, N., Bahmanpour, A., Yamada, S. and Liu, B. A., 2010. Shaking model tests on mitigation of liquefaction-induced ground flow by underground columns. International Symposium on Recent and Future Technologies in Coastal Development, CD-ROM.

Yamamoto, Y., Takahashi, N., and Kurokawa, Y., 2006. Analytical Study on the Liquefaction Countermeasure Effect of the Pile Type Deep Mixing Method. Reports of technical research institute of Sumitomo Mitsui Construction Co., Ltd., No. 4, pp. 45-53. (In Japanese)

Yasuda, S., Murasawa, Y., Konishi, T., Tanaka, T., and Uchiyama, J., 2003. Effect of soil-cement column with a triangular grid pattern as a countermeasure against liquefaction. Proceedings of the 38th Japan National Conference on Geotechnical Engineering, pp.1881-1882. (In Japanese)